

An adaptive finite element multigrid solver using GPU acceleration

M. Liebchen^{*} U. Kaya[†] C. Lessig[‡] T. Richter[§]

May 9, 2024

Adaptive finite elements combined with geometric multigrid solvers are one of the most efficient numerical methods for problems such as the instationary Navier-Stokes equations. Yet despite their efficiency, computations remain expensive and the simulation of, for example, complex flow problems can take many hours or days. GPUs provide an interesting avenue to speed up the calculations due to their very large theoretical peak performance. However, the large degree of parallelism and non-standard API make the use of GPUs in scientific computing challenging. In this work, we develop a GPU acceleration for the adaptive finite element library Gascoigne and study its effectiveness for different systems of partial differential equations. Through the systematic formulation of all computations as linear algebra operations, we can employ GPU-accelerated linear algebra libraries, which simplifies the implementation and ensures the maintainability of the code while achieving very efficient GPU utilizations. Our results for a transport-diffusion equation, linear elasticity, and the instationary Navier-Stokes equations show substantial speedups of up to 20X compared to multi-core CPU implementations.

1 Introduction

The combination of adaptive finite elements and geometric multigrid solvers is one of the most efficient approaches for the numerical approximation of partial differential equations. Adaptive mesh refinement schemes based on numerical a posteriori error estimates allow for optimal refinement [33] while geometric multigrid solvers provide the solution to the arising linear systems of equations in linear complexity. For many partial differential equations, the combination yields an overall approach with optimal computational complexity for a prescribed accuracy.

The mathematical and computational optimality come at the price of complex algorithms and a lack of regular structure in the computations. This is due to the adaptivity of the discretization, resulting in an irregular mesh and stencils, and the multi-scale nature of the

^{*}Institute of Analysis and Numerics, OVGU Magdeburg, Germany (manuel.liebchen@ovgu.de).

[†]Institute of Analysis and Numerics, OVGU Magdeburg, Germany (utku.kaya@ovgu.de).

[‡]European Centre for Medium-Range Weather Forecasts (christian.lessig@ecmwf.int).

[§]Institute of Analysis and Numerics, OVGU Magdeburg, Germany (thomas.richter@ovgu.de).

solvers. Furthermore, memory is often addressed in an unstructured way, hampering the parallelization of the computations.

These challenges are one of the central reasons that parallel accelerator co-processors, such as GPU's and TPU's, are still only rarely used in numerical simulations, including for adaptive multi-grid methods. Accelerators are highly attractive since the computational power of CPUs has stagnated in the last decade while those accelerators has increased dramatically.

Accelerators use task- and data-parallelism as well as specialization to achieve a very large peak performance. While a high degree of parallelism is inherent in some problems, e.g. in computer graphics and deep learning, it poses challenges for the implementation of adaptive algorithms in numerical linear algebra and scientific computing. This holds true in particular for data-parallelism that requires regular, structured computations with uniform memory access patterns. One direction to address this gap is by changing to algorithms with highly regular computations, such as lattice Boltzmann methods in fluid mechanics [25, 27]. A minimally invasive use of GPU's in classical finite element simulation tools is also possible but yields little to no acceleration [14].

Another challenge for the the use of accelerator hardware in scientific computing is that these are optimized for single, half or even less precision while double precision remains the standard for most calculations in numerical mathematics. In [29], this is addressed by using a hierarchical approach to modify the linear systems, denoted as pre-handling. An alternative direction is the use of machine learning methods, especially deep neural networks, in the context of simulations, which can be executed very efficiently and in lower precision on accelerator hardware with speedups up to several orders of magnitude, e.g. [7].

For algebraic multi-grid methods, GPU accelerated libraries exist, e.g. amgx [22] and ginkgo [1]. However, these are likely less efficient than geometric multi-grid methods, if applicable.

The integration of GPU's into an existing geometric multigrid solver was already presented in [15]. The obtained speedup were moderate but the work describes how a transparent implementation into an existing software can be achieved. The consequences of mixed precision arithmetic were also discussed in this work. In [13], the same authors presented a geometric multigrid method that is based entirely on sparse matrix-vector multiplications and can thus be easily and efficiently implemented on different hardware using suitable libraries. Applied to stationary linear differential equations, an acceleration of the overall solver by a factor of up to 5 was achieved compared to CPU systems. In [17], the authors investigate the GPU parallelization of several smoothers within a matrix-based geometric multigrid method. The implementation allows for locally refined unstructured meshes, but, the obtained speedup is limited and does not substantially exceed that of multi-core CPU's. NVIDIA [32] has presented a highly efficient geometric multigrid solver for 3d linear elliptic problems. It reaches very high throughput and demonstrates the potential of native CUDA implementations. It is, however, limited in terms of flexibility and its applicability to unstructured meshes.

In this article, we show that highly efficient adaptive finite elements with local multigrid solvers can be implemented efficiently on GPU accelerators without limiting the flexibility of the method. For this, we formulate computations as matrix-vector and matrix-matrix computations. This allows us to use the cuBLAS and cuSPARSE libraries [24] that are highly optimized while the code remains close to those with BLAS calls on the CPU. Hence, the CPU and GPU versions can retain the same structure and differ only in the linear algebra function calls and additional CPU-to-GPU memory transfer in the GPU version. It, nonetheless, allows for the use of custom CUDA kernels when necessary and we demonstrate that the use of simple

native CUDA code can provide significant speedups for operations that do not naturally map to (sparse) linear algebra. Due to these optimizations, the largest performance bottleneck comes from the memory transfer between CPU and GPU. In our final code, large parts of the computations have been transferred to the GPU and thus the slowdown through the transfer is also small.

We demonstrate the generality and flexibility of our approach by applying it to two linear elliptic problems, namely the transport-diffusion equation in 2d and a 3d linear elasticity problem. The discretization of these two equations results directly in a linear system of equations that can be approximated with the GPU-accelerated geometric multigrid solver. As a third example, we consider the instationary Navier-Stokes equations. For these, we first derive an explicit pressure-correction method, which can be represented by matrix-vector multiplications and a pressure-Poisson problem, the latter one being solved with the multigrid solver. Special attention is given to the nonlinearity of the Navier-Stokes equations. Through a reformulation, also this will be approximated by a product with a pre-computed sparse matrix on the GPU. For all three examples, we obtain significant speed-ups between 5X and 20X for our final GPU parallelizations. At the same time, the systematic use of (sparse) linear algebra leads to easily understandable and maintainable code for the GPU computations.

Outline The remainder of the article is structured as follows. In Sec. 2 we introduce the mathematical notation and briefly present the finite element discretization. There, we also describe the geometric multigrid method. In Section 3, we will discuss accelerators such as GPUs and describe the specifics of the hardware and how they need to be reflected in the algorithms. We also introduce software libraries that facilitate the use of accelerator hardware. Section 4 describes our implementation of the multigrid process based on the cuSPARSE library [24]. Finally, in Section 5, we present numerical test problems and discuss the results. We conclude in Section 6.

2 Adaptive Finite Element Discretization and Multigrid Solver

2.1 Finite element discretization

We denote a domain by $\Omega \subset \mathbb{R}^d$, where $d = 2$ or $d = 3$ is the dimension. By Ω_h we denote a finite element mesh consisting of N_h quadrilaterals or generalized (allowing curved faces) hexahedras. The elements $T \in \Omega_h$ all arise from a reference element \hat{T}

$$\hat{T}_T : \hat{T} \mapsto T$$

that is the unit square in 2d and the unit cube in 3d. We will consider isoparametric finite elements, where the mapping itself comes from the finite element space. Let

$$Q^r := \{x_1^{\alpha_1} \cdots x_d^{\alpha_d}, \alpha_i \in \mathbb{N}, 0 \leq \alpha_i \leq r\}$$

be the space of polynomials of maximal degree r in each coordinate. Then, $\hat{T}_T \in [Q^r]^d$ and we define the finite element spaces of degree r as

$$V_h^{(r)} := \{\phi \in C(\bar{\Omega}) : \phi \circ T_T^{-1} \in Q^r \quad \forall T \in \Omega_h\}.$$

We assume shape regularity in the sense that $\|\nabla T_T\| \cdot \|\nabla T_T^{-1}\| \leq c$ uniform in $h > 0$, see [28, Sec. 4.2]. Structural regularity is relaxed by allowing local mesh refinement with at most 1

Algorithm 2.1: Geometric multigrid solver

Given a hierarchy of meshes Ω_l and corresponding finite element spaces \mathbf{V}_l for $l = 0, \dots, L$ and an initial value $x_L^0 \in \mathbf{V}_L$. For $n = 1, \dots, N_{max}$ iterate

$$x_L^{(n)} = GMG(L, x_L^{(n-1)}, b_L)$$

where $GMG(l, x_l, b_l)$ is recursively defined as:

Step 0: Coarse mesh problem	if $l = 0$ return $A_0^{-1}b_0$
Step 1: Pre-smooth	$x'_l = \mathcal{S}_l(x_l, b_l)$
Step 2: Restrict residual	$d_{l-1} = \mathcal{R}_{l-1}(b_l - A_l x'_l)$
Step 3: Recursive coarse mesh correction	$y_{l-1} = GMG(l-1, 0, d_{l-1})$
Step 4: Prolongate update	$x''_l = x'_l + \mathcal{P}_{l-1}y_{l-1}$
Step 5: Post-smooth	return $\mathcal{S}_l(x''_l, b_l)$

hanging node per face, again, see [28, Sec 4.2] for the specific realization in the finite element library Gascoigne 3d [10].

Systems or partial differential equations such as the Navier-Stokes equations or elasticity will be discretized with equal-order finite elements, i.e. $\mathbf{V}_h = [V_h^{(r)}]^c$, where $c \in \mathbb{N}$ is the number of components. Gascoigne 3d combines these components locally. Taking the 3d Navier-Stokes equations as example this means that the vector is represented as a matrix with entries $x_{i,c}$ where i refers to the grid node and c to the component ($c = 1$ pressure, $c = 2, 3, 4$ velocities). The system matrix also has double indexing. Each matrix entry A_{ij} is itself a (dense) matrix $A_{ij} \in \mathbb{R}^{n_c \times n_c}$ with $n_c = 4$ in the case of 3d Navier-Stokes. Basis functions are always scalar, such that a Navier-Stokes solution is given as

$$\begin{pmatrix} p_h(x) \\ \mathbf{u}_h(x) \end{pmatrix} = \sum_{i=1}^N \begin{pmatrix} x_{i,1} \\ x_{i,2} \\ x_{i,3} \\ x_{i,4} \end{pmatrix} \phi_h^i(x).$$

Keeping the solution components together is beneficial in terms of cache efficiency for problems where one obtains large system matrices like Navier-Stokes ($c = 4$) or 3d elasticity, where $c = 6$ when the velocity and deformation fields are combined [8]. The memory layout of this approach is not easily transferred to GPUs as standard libraries like cuSPARSE do not support such blocked matrices. Section 4.1.1 will give details.

2.2 Adaptivity and geometric multigrid hierarchy

Adaptivity of the computations is realized by means of hierarchical local mesh refinement. If an element $T \in \Omega_h$ is chosen for refinement, it is replaced by 4 elements in 2d and 8 elements in 3d. We allow a level jump of 1 for neighboring elements. Refinement of one element can therefore lead to adjacent further refinements. On edges and faces with a level jump, interior degrees of freedom, so-called hanging nodes, are replaced by the interpolation from the neighboring indices. These interpolations are realized by matrix-vector products with sparse matrices that depend on the mesh structure and the chosen finite element degree. Mesh refinement can be

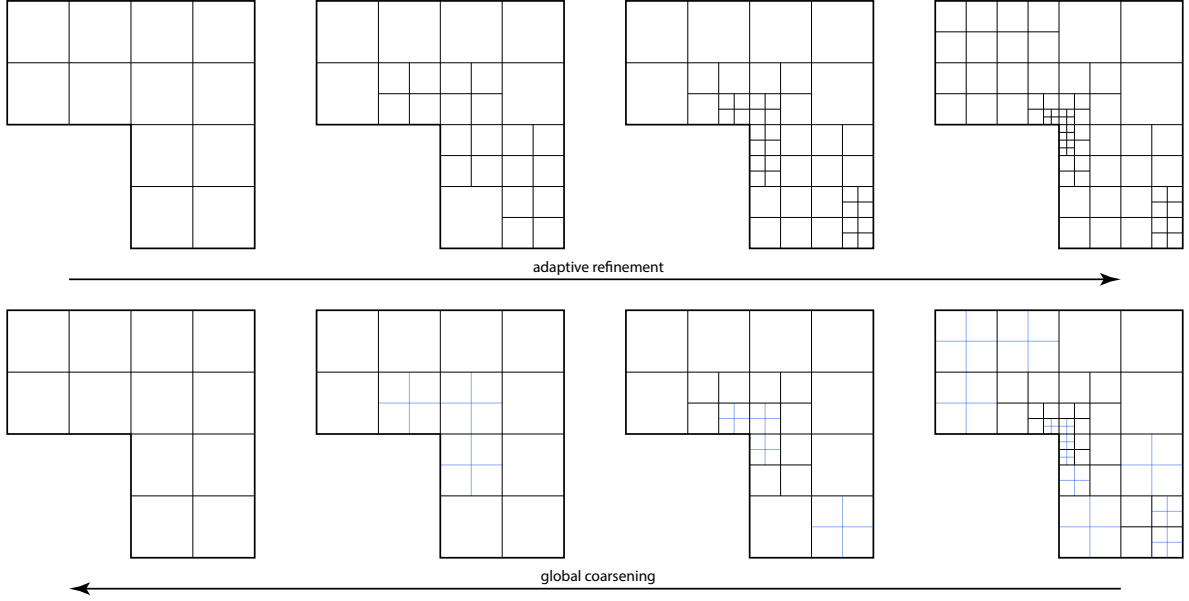


Figure 2.1: Top row: hierarchy of adaptively refined 2:1 meshes with hanging nodes. Bottom row: global coarsening resulting in the multigrid hierarchy. In each step as many refinements are taken back as possible (shown in blue) for a rapid decrease of the mesh complexity.

based either on a priori knowledge or on a posteriori error estimates, the latter usually in the context of the dual weighted residual method [6, 9].

Successive mesh refinement results in a hierarchy of meshes. Instead of using this hierarchy for the setup of the geometric multigrid solver, we start with the finest mesh $\Omega_h =: \Omega_L$ and recursively coarsen it until we reach a coarse mesh $\Omega_H =: \Omega_0$ with small complexity N_H . In each coarsening step, as many refinements as possible are taken back, yielding a hierarchy $\Omega_h = \Omega_L \succeq \Omega_{L-1} \succeq \dots \Omega_0 = \Omega_H$. We follow a global multigrid approach where each intermediate level Ω_l spans the complete domain, see [4]. Fig. 2.1 provides a sketch of the adaptive mesh refinement and the global coarsening procedure that result in two different hierarchies of meshes.

The multigrid solver is the standard V -cycle. Coarse mesh problems are either solved exactly or approximated using a couple of smoothing steps. The geometric multigrid iteration is either used as linear solver or as pre-conditioner in a GMRES solver [30]. The GMRES solver is more robust and usually required for problems that are transport dominated or when meshes with large element aspect ratios are used.

3 Data-parallel accelerators

Accelerator co-processors, such as GPUs from NVIDIA and AMD and TPUs from Google, are used in a wide range of applications, such as computer gaming and neural networks training. Due to their very large compute power, they also play an increasingly important role in scientific computing. The large compute power is achieved through a very high degree of parallelization

as well as specialization. For example, NVIDIA’s GPUs combine MIMD parallelism with up to 128 streaming multi-processors with data-parallelism with a logical, pipelined width of 1024 and a hardware width of 32 (and 8 on the latest hardware). Additionally, significant compute power is provided by dedicated matrix-matrix multiplications engines known as tensor cores and introduced for neural network training. Accelerator co-processors also differ from conventional processors through native hardware support of lower precision data types such as half precision and even 8-bit computations on the latest generation of chips. Accelerator co-processors as used in this work come with their own, dedicated memory hierarchy starting from a RAM, and with typically two layers of caches. To perform computations on the accelerator, data hence needs to first be transferred to the accelerator RAM through a comparatively slow memory interface.

The programming of accelerator hardware is typically challenging due to the high degree of parallelism and narrow “fast paths” on the hardware (e.g. because of smaller caches compared to CPUs) that are difficult to optimize for and can change from hardware generation to hardware generation. This is compounded by the separate memory hierarchy on the accelerator and the slow interface to CPU RAM, that can easily become a bottleneck. Furthermore, native software libraries, such as CUDA and ROCm, are usually vendor specific and not standardized, with often also an incomplete documentation. This makes their use by non-experts challenging and leads to a high maintenance effort when always the latest features should be used.

Different libraries have been proposed to aid with the development of GPU-accelerated software. OpenACC and OpenMP provide pragma-based access to the compute power of GPUs that is very simple to use but also limited in the potential for optimizations. SYCL [34] and Kokkos [36] provide a middle-ground with more complex usage but also more flexibility. Machine learning libraries such as PyTorch [26] and jax [11] follow a new paradigm for GPU programming where the application code is specified in a high-level language and a backend, such as XLA [31] or ATen [26], generates highly efficient, hardware-specific code. This concept is sometimes also referred to as domain-specific language, e.g. [21]. Recently, Triton [35] was proposed as a complement to existing machine learning libraries. It still allows for highly simplified programming of accelerators compared to CUDA and ROCm but provides more control than PyTorch and jax, and hence typically yields more efficient code.

For specific applications, such as linear algebra or discrete Fourier transform, also highly optimized libraries exist. These provide very high performance while, through the targeted use case, also allow for much simpler usage than, e.g., CUDA. In our work, we will build on a linear algebra formulation of our adaptive PDE solvers. This allows us to use the cuBLAS [23] and cuSPARSE libraries [24] that provides high performance while being simple to use with a software interface that is roughly comparable to those of the conventional BLAS library. Furthermore, cuBLAS and cuSPARSE can still be combined with native CUDA code when necessary, i.e. when an operation cannot be expressed efficiently in linear algebra.

4 CUDA multigrid

In this section we discuss our extension of the adaptive finite element library Gascoigne 3d to use GPU accelerators for a wide range of computations. The extensions have been designed with two use cases in mind: first, non-stationary but linear systems of partial differential equations, where a single system matrix is reused in every time step or at least in many time steps, and, second, nonlinear problems that can be formulated in terms of fixed matrices that

Algorithm 4.1: Nonstationary Linear Problem

```

Basic Initialization;                                     // init
1 Assemble Matrices;                                     // init
2 CopyToGPU(Matrix);                                     // copy
3 for time-iter do
4   Assemble Right Hand Side;                             // rhs
5   CopyToGPU(RighHandSide);                             // copy
6   SolveLinearProblem;                                   // solve
7 end
8 CopyFromGPU(Solution);                                 // copy
9

```

Algorithm 4.2: Explicit Navier-Stokes Pressure Correction

```

Basic Initialization
Assemble Matrices
CopyToGPU(Matrix);                                     // copy
10 for time-iter do
11   Assemble Momentum right Hand Side;                   // mom-rhs
12   Explicit Solve Momentum Problem;                     // mom-solve
13   Assemble Pressure Right Hand Side;                   // pres-rhs
14   for GMRES iteration do
15     Multigrid Pressure ;                               // pres-solve
16   end
17   Update Pressure;                                     // pres-up
18   Correct Velocity
19 end
20 CopyFromGPU(Solution);                                 // copy
21

```

do not need re-assembly. The second cases includes a pressure-projection based solvers for the nonstationary nonlinear Navier-Stokes equations but can be extended to more complex flow problems such as the Boussinesq approximation [12]. Both problem classes have in common that matrices are assembled only once and the complete workflow can be formulated in terms of matrix vector products and the solution of linear systems of equations. Algorithms 4.1 and 4.2 show the typical workflow for the problem types. Computations highlighted in blue are completely performed on the GPU, orange marks transfer of data between GPU and CPU.

It is no fundamental issue to also port the computations of general nonlinear problems to a GPU. However, keeping the flexibility and support of different discretizations and triangulations is not as easily handled for the ill-structured setup of typical finite element assemblies of system matrices and residuals in the general nonlinear case. We hence defer this to future work.

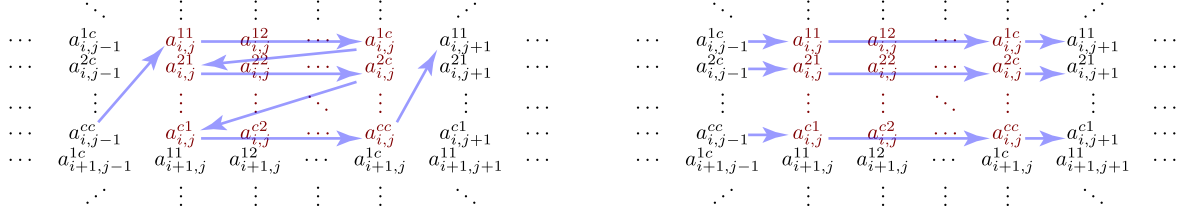


Figure 4.1: Storage of matrix on CPU (left) and GPU (right). While we employ a block-wise ordering of the matrix entries on the CPU and cluster the $c \times c$ components of a system of PDEs on the CPU, the entries are stored in standard CSR format on the GPU.

4.1 General architecture

Our principal approach for the CUDA parallelization of Gascoigne 3d is to formulate all operations in terms of (potentially sparse) matrix-vector and matrix-matrix products and to realize these with the highly optimized cuBLAS [23] and cuSPARSE [24] libraries. This approach differs from the existing implementation in Gascoigne 3d where many operations such as the handling of hanging nodes or the multigrid mesh transfer are based on the local connectivity of the degrees of freedom as function of mesh and discretization. However, this functionality can easily be realized as matrix-vector products, including for the handling of hanging nodes and all mesh transfer operations. This is, e.g., the approach taken from the outset in the deal.II finite element library [2].

All high level operations in Gascoigne 3d are performed on abstract interface classes to vectors and matrices to allow for MPI parallelization [20, 5]. This has been retained in the CUDA-version so that the high-level control flow and complex algorithms (such as Newton, multigrid, GMRES) are unchanged since they only operate on the interfaces. The approach minimizes the changes that were overall required and allows to flexibly retain both the CPU and the GPU backend.

4.1.1 Storage

Gascoigne 3d uses a block-wise memory concept in which the various components of a partial differential equation (e.g. the 3 deformation unknowns in 3d solid mechanics or the pressure and the three velocity components in fluid mechanics) are stored next to each other. Matrices are double-indexed and the outer index (i, j) refers to the mesh node yielding the entry $a_{i,j} \in \mathbb{R}^{c \times c}$ that stores (aligned in memory) the local couplings between the solution components as a matrix. In general, this setup helps to efficiently use caching [8, 20]. Using cuSPARSE this block-matrix format is not supported. While vectors are directly transferred to the GPU using the same memory layout, the inner matrix blocks must be resolved and matrices are stored in the usual CSR format. Fig. 4.1 shows a visualization of the matrix storage concept on the CPU (left) and the GPU (right).

The representation of a matrix in GPU memory is directly allocated when the matrix is created and assembled on the CPU. This helps to better exploit the asynchronous data transfer. Our implementation is directed at problems where the matrix stays fixed such that this transfer is required just once. For vectors, the data transfer takes place when a `cudaActivate()`

function is called on the object owning the data, e.g. a class steering the multigrid solver. Data is transferred back to the CPU when the corresponding `cudaDeactivate()` function is called.

4.1.2 Mapping (sparse) linear algebra to the GPU

The matrix-matrix and matrix-vector multiplications that are the essential building blocks of CUDA-Gascoigne 3d are realized with cuBLAS and cuSPARSE, which provide an interface in close analogy to BLAS. For example, the function `cuSPARSESpMV` performs for a sparse version of BLAS's `gemv`, i.e. it computes $\alpha \text{op}(A)x + \beta y$ where α, β are scalar, x, y are vectors and A is a matrix. The approach reduces the implementation effort for our GPU-parallelization substantially and ensures it is maintainable, i.e. further developments of Gascoigne 3d can be implemented without substantially efforts also for the GPU version.

4.1.3 Custom CUDA kernels

Almost all operations required for the adaptive finite element solvers of Gascoigne 3d can be expressed efficiently using linear algebra. However, we found some exceptions and performing these calculations on the CPU incurred a very high penalty due to the required data transfer between GPU and CPU. We therefore implemented small parts of the computations in native CUDA, which avoided the extra memory transfers and hence the penalty. This is facilitated by cuBLAS and cuSPARSE operating on raw CUDA pointers in device memory which can directly also be used in native CUDA. Details of the implementation are given in Sec. 5.3.

The flexibility to combine cuBLAS, cuSPARSE and native CUDA is, in our opinion, an important feature to avoid CPU-GPU data transfer and to be able to flexibly implement algorithms with CUDA-Gascoigne-3d. The total number of required custom kernels is very small and serves as guideline for measuring the effort to port further applications to the GPU.

4.1.4 Geometric Multigrid CUDA

As a concrete example, we describe in the following how geometric multi-grid algorithm in Algo. 2.1 is realized in CUDA-Gascoigne-3d. All computations are entirely performed on the GPU. Hence, data transfer overhead is incurred only at the beginning and end of the computations, see also Algorithm 4.1 and 4.2.

All steps of the algorithm involve only elementary operations that can directly be formulated in cuSPARSE or cuBLAS. Mostly, matrix-vector products must be computed, e.g. for prolongation and restriction, but also for the smoother. To avoid memory transfer between CPU and GPU it is essential that the smoother can be performed completely on the GPU. At the moment we limit ourselves to very simple smoothers of Jacobi or block-Jacobi type that can be written as

$$x^{(l+1)} = x^{(l)} + \omega S(b - Ax^{(l)}),$$

where $\omega \in \mathbb{R}$ is a damping factor and $S \in \mathbb{R}^{n \times n}$ the smoothing operator, written as fixed matrix. More complex smoothers can, in principle, be implemented using native CUDA but we leave this to future work.

Mesh transfer operations are usually done locally. In the hierarchical setup of finite elements on quadrilateral or hexahedral meshes, prolongation of a solution to the next finer mesh is the usual embedding. To illustrate this, let K be an element of the coarse mesh Ω_l and K_1, \dots, K_p be the resulting fine elements on level Ω_{l+1} , where $p = 2^d$ with d being the spatial dimension.

Considering finite elements of degree r , $(r+1)^d$ unknowns are involved on mesh level l and $(2r+1)^d$ on level $l+1$. Prolongation is then by means of

$$u_i^{(l+1)} = \sum_{j=1}^{(r+1)^d} \chi_{ij} u_j^{(l)}, \quad i = 1, \dots, (2r+1)^d. \quad (1)$$

The $(r+1)^d \times (2r+1)^d$ coefficients χ_{ij} are the same for each mesh element. (1) can be written as one global matrix-vector product

$$u_h^{(l+1)} = P_l u_h^{(l)}$$

with $P_l \in \mathbb{R}^{N_{l+1} \times N_l}$ and its entries given by χ_{ij} . With the number of distinct elements in P_l being very small, the use of the matrix formulation would be sub-optimal on the CPU. On the GPU, however, it is performant and allows us to use cuSPARSE. The multigrid restriction $R_l : \Omega_{l+1} \rightarrow \Omega_l$ is the transpose of the prolongation, i.e. $R_l = P_l^T$ and hence also implemented using a sparse matrix in cuSPARSE. Similarly to the mesh transfer, also for hanging nodes we formulate the operations for averaging and distributing the values of the solution vector as sparse matrix-vector products, compare Section 2.2.

The coarse mesh problem in **Step 0** of Algorithm 2.1 is not solved directly. Instead, we simply apply several steps of the smoothing iteration such that no additional infrastructure for GPU parallelization is required.

4.1.5 GMRES as linear solver on the GPU

For reasons of numerical stability, e.g. on non-uniform meshes, the multigrid iteration can often not be used directly as linear solver. They are then employed as preconditioner in a GMRES iteration. Our GMRES solver follows the approach described in [30, Section 6.5.3], using the modified Gram Schmidt algorithm for orthogonalization and Givens rotation for solving the resulting overdetermined linear system. Due to the multigrid preconditioning, we avoid stability issues in the Gram Schmidt orthogonalization and never have to perform more than 5-10 GMRES steps. The Gram Schmidt iteration is also completely run on the GPU using cuSPARSE and cuBLAS operations. As a maximum of $n_G \leq 10$ steps is usually performed, the resulting overdetermined system used to find the GMRES solution is very small and its step-wise transformation to a diagonal matrix with Givens rotations is performed on the CPU. The size of this matrix does not exceed $\mathbb{R}^{(n_G+1) \times n_G}$ such that memory transfer between GPU and CPU is negligible. Details are given in [30].

5 Results

In this section, we present several applications where we employ the GPU-accelerated multigrid method presented in the last section. We start with two linear elliptic problems, namely the transport-diffusion equation in 2d and a 3d linear elasticity problem. The discretization of these two equations results directly in a linear system of equations that can be approximated with the geometric multigrid solver and falls into the class of systems handled by Algorithm 4.1.

As a third example, we consider the Navier-Stokes equations. For these, we first derive an explicit pressure-correction method, which can be represented by matrix-vector multiplications and a pressure-Poisson problem, latter one being solved with the multigrid solver. Special

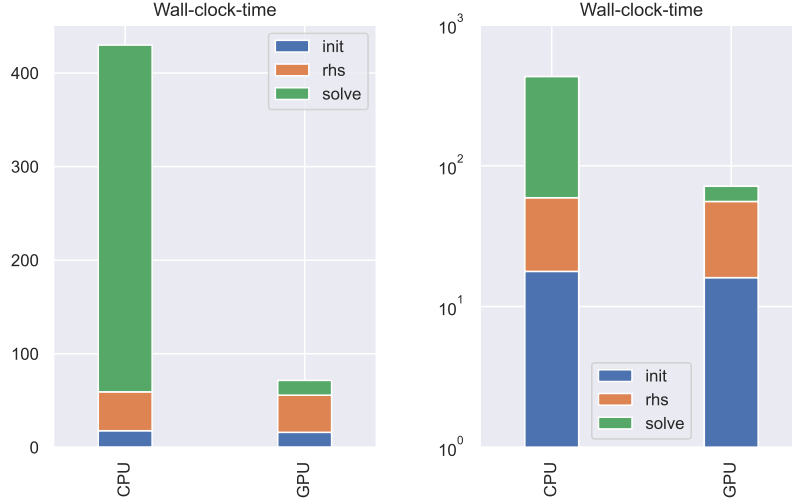


Figure 5.1: Transport-diffusion equation: Wall-clock times CPU vs. GPU on the finest mesh level with 1 000 000 degrees of freedom (linear scale on the left and logarithmic on the right).

attention is given to the nonlinearity of the Navier-Stokes equations. Through a reformulation, also this will be approximated by a product with a pre-computed sparse matrix and can easily be performed on the GPU.

If not noted otherwise, all CPU computations are carried out on an Intel Xeon E5-2640 running at 2.40 Ghz using 8 threads. The GPU computations are performed on the same machine using an Nvidia V100 card with 16 GB of GPU RAM. When using the GPU to accelerate the multigrid solver, those parts of Gascoigne that reside on the CPU still run on 8 parallel threads. We always indicated wall-clock times and separately specify the different contributions of Algorithms 4.1 and 4.2.

5.1 Transport-diffusion equation

Let $\Omega \in (0, 1)^2$ and $I = (0, T]$ with $T = 2$. On $I \times \Omega$ we find θ subject to the following transport-diffusion problem

$$\partial_t \theta - \lambda \Delta \theta + (\mathbf{b} \cdot \nabla) \theta = f \quad \text{in } (0, T] \times \Omega, \quad (2)$$

$$\theta = \theta_b \quad \text{on } (0, T] \times \partial\Omega, \quad (3)$$

$$\theta(0, x, y) = \theta_0 \quad \text{in } 0 \times \Omega. \quad (4)$$

where $\lambda = 0.01$ and $\mathbf{b} = (0, -1)^T$. The source term f , boundary condition θ_b and initial condition θ_0 are chosen such that equations (2) - (4) have the exact solution

$$\theta_{ex}(t, x, y) = \exp\left(-\frac{1}{4}(m(t, x)^2 + m(t, y)^2)\right), \quad m(t, z) = \frac{1}{2} + \frac{1}{4} \cos\left(\frac{\pi}{2}t\right) - z.$$

We consider the backward Euler method with a time-step size $\Delta t = 0.02$. Uniform quadrilateral spatial meshes with a range of sizes given by h^{-n} where $n \in \{4, \dots, 10\}$ are used to demonstrate the scaling efficiency of the GPU accelerated version. Hence, on the coarsest mesh the problem

has $4^4 = 256$ degrees of freedom whereas the finest mesh comprises $4^{10} \approx 1\,000\,000$ degrees of freedom. In each of the $T/\Delta t = 100$ time steps, a linear system must be solved. To ensure the robustness of the method, we use the GMRES solver, preconditioned with multigrid, to approximate the linear problems, cf. Sec. 4.1.5. Fig. 5.1 shows the wall-clock times comparing the CPU and GPU implementations on the finest mesh level. The labels **init**, **rhs** and **solve** refer to the initialization (mainly assembly of system matrix), to the computation of the right hand side, and to the actual solution, respectively. Matrix assembly and the computation of the right hand side involve numerical quadrature over the mesh elements which is not ported to the GPU. Hence, no speedup is observed. The time for solving the linear problems, however, is reduced from 370 s on the CPU to 15.7 s on the GPU, a factor of about 24; see also Table 5.1 for the raw data. For large problems, the non-accelerated assembly of the right hand side **rhs** hence becomes dominant. In Section 5.3 we describe how this term can be efficiently transferred to the GPU by using mass lumping.

mesh level	DOFs	CPU				GPU			
		init	rhs	solve	sum	init	rhs	solve	sum
6	4 096	0.11	0.23	1.28	1.62	0.42	0.21	1.93	2.55
7	16 384	0.36	0.70	4.44	5.51	0.66	0.68	2.56	3.90
8	65 536	1.23	2.45	18.92	22.6	1.52	2.52	3.73	7.76
9	262 144	4.46	10.39	85.03	99.87	4.48	9.93	5.94	20.35
10	1 048 576	17.78	41.54	370.51	429.82	16.05	39.74	15.73	71.52

Table 5.1: Transport-diffusion problem: wall clock times on CPU and GPU in seconds.

In Figure 5.2 we visually analyze the performance of the CPU (using 8 threads) and GPU version of Gascoigne 3d on the sequence of uniformly refined meshes ranging from $h = 2^{-4}$ to $h = 2^{-10}$. While the scaling of all components **init**, **rhs** and **solve** is linear on the CPU, the GPU-accelerated linear solver **solve** benefits from larger problems. This is in line with theoretical considerations since the very large degree of parallelism and the very deep pipelining on the GPU requires large problems to fully utilize the computational units.

5.2 Linear elasticity

As second problem we consider the linear elasticity equation

$$\partial_t^2 \mathbf{u} - \operatorname{div} \boldsymbol{\sigma}(\mathbf{u}) = \mathbf{f} \quad \text{in } (0, T] \times \Omega, \quad (5)$$

on the domain $\Omega = (0, 1)^3$ in the time interval $I = [0, 2.5]$. By \mathbf{u} we denote the displacement, $\mathbf{f} = (0, -1, 0)^T$ is the right hand side vector and the stress tensor is given by

$$\boldsymbol{\sigma}(\mathbf{u}) = \lambda \operatorname{tr}(\boldsymbol{\epsilon}(\mathbf{u})) \mathbf{I} + 2\mu \boldsymbol{\epsilon}(\mathbf{u}), \quad \boldsymbol{\epsilon}(\mathbf{u}) = \frac{1}{2}(\nabla \mathbf{u} + \nabla \mathbf{u}^T)$$

where \mathbf{I} is the identity tensor, tr is the trace operator on a tensor and $\lambda = 8 \cdot 10^4$ and $\mu = 2 \cdot 10^4$ are the Lamé parameters. Eq. (5) can be written as two coupled PDEs with first order time

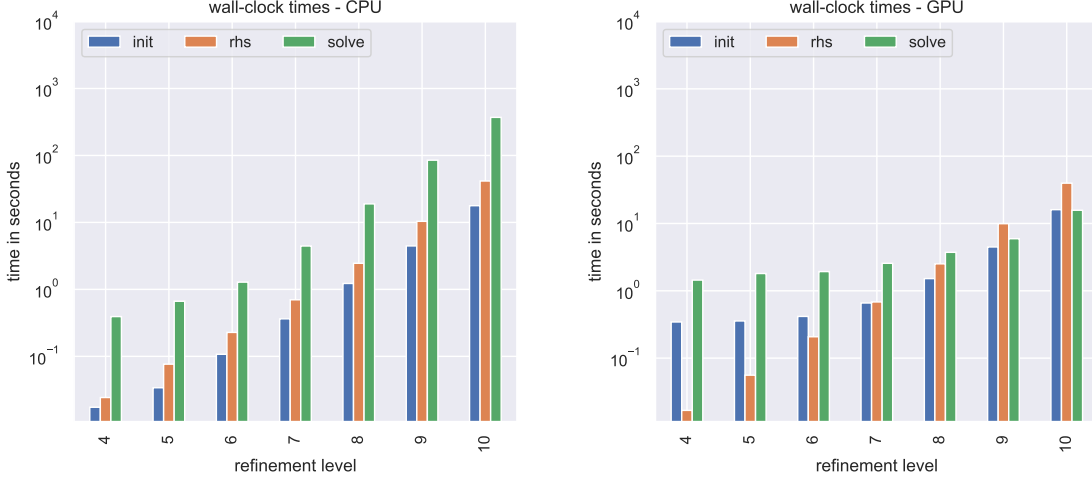


Figure 5.2: Transport-diffusion equation: Wall-clock times CPU vs. GPU on a sequence of uniformly refined meshes.

derivatives,

$$\partial_t \mathbf{u} - \mathbf{v} = \mathbf{0} \quad \text{in } (0, T] \times \Omega \quad (6)$$

$$\partial_t \mathbf{v} - \operatorname{div} \boldsymbol{\sigma}(\mathbf{u}) = \mathbf{f} \quad \text{in } (0, T] \times \Omega, \quad (7)$$

with homogenous Dirichlet boundary conditions and zero initial conditions for \mathbf{u} and \mathbf{v} .

We use this test case to illustrate the performance of the CUDA multigrid solver on adaptively refined meshes, see Fig. 5.3 for a visualization of the used mesh. Adaptive refinement is not driven in a problem specific way here but we consider typical cases of adaptive meshing, namely refinement towards a complete face of the box, refinement towards an edge, and refinement towards a vertex. This mimics resolving singularities that have a 2d pattern (face), a 1d pattern (edge) and a 0d pattern (vertex). Table 5.2 lists the number of mesh nodes and the fraction of mesh nodes that are hanging. The number of degrees of freedom is six times this number of mesh nodes as we have 3 deformation and 3 velocity components. Hanging nodes do not improve the approximation property but instead disrupt the structure of the problem by distorting the sparsity pattern of the matrix.

For time discretization of (6)-(7) the backward Euler method is used with a step size of $\Delta t = 0.025$ resulting in $2.5/\Delta t = 100$ time steps.

We provide a detailed discussion of the intermediate case, the refinement towards one edge. Fig. 5.4a gives the timings on the finest mesh level (34 985 nodes, hence 209 910 degrees of freedom, about 25 600 of them in hanging nodes) for the CPU version and the GPU version. As for the transport-diffusion equation, times for initialization `init` and right hand side `rhs` do not change, as these parts are not implemented on the GPU. The computation time for the linear solver is, however, drastically reduced, compare Table 5.3b. On the finest mesh, the solution time reduces from 1529s to 96s, i.e. by a factor of 16. As the time for matrix assembly (`init`) and computing the right hand side (`rhs`) are negligible, the overall speedup is still close to 14 (compared to about 13 for the transport-diffusion problem on a much finer mesh).

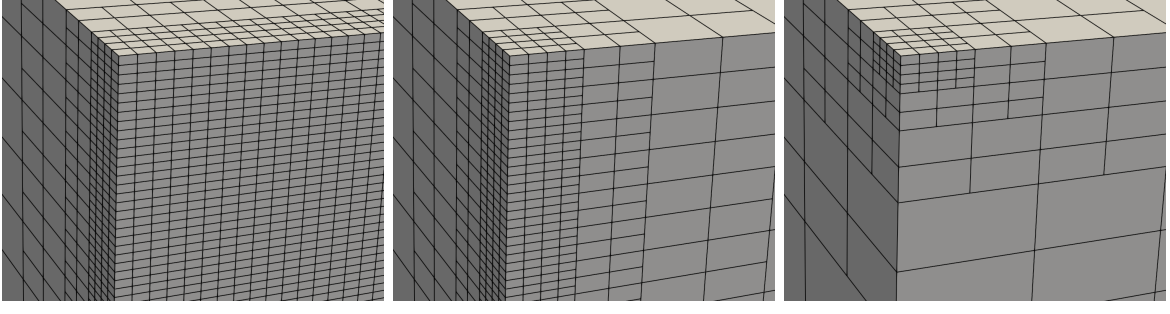


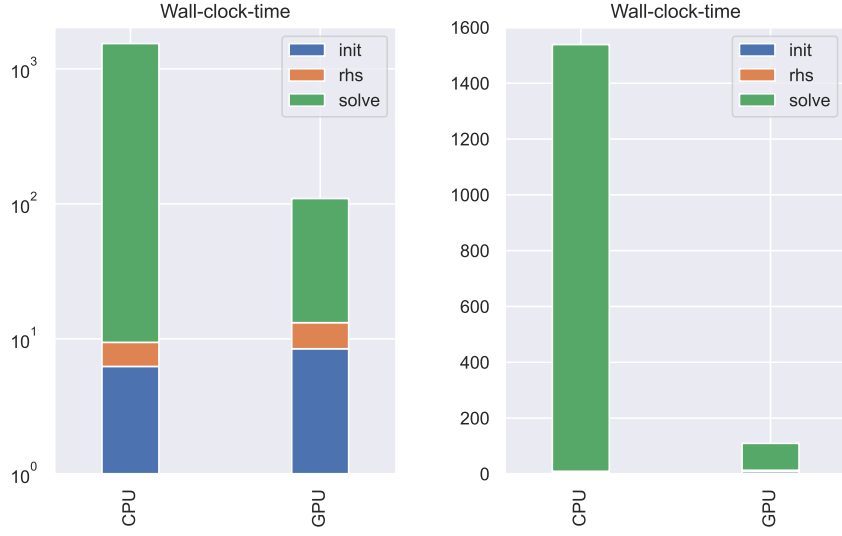
Figure 5.3: Visualization of the adaptive meshes. From left to right: Refinement towards one face, towards an edge, and towards one vertex. The fraction of hanging nodes and hence of unstructuredness increases from the left to the right.

Mesh levels	1	2	3	4	5	6
Face	729	2 925	11 281	43 861	172 505	683 741
	0.00%	4.92%	6.10%	6.33%	6.45%	6.46%
Edge	729	1 881	4 129	8 569	17 393	34 985
	0.00%	7.66%	10.3%	11.4%	11.9%	12.2%
Vertex	729	1 333	1 937	2 541	3 145	3 749
	0.00%	8.10%	11.2%	12.8%	13.7%	14.4%

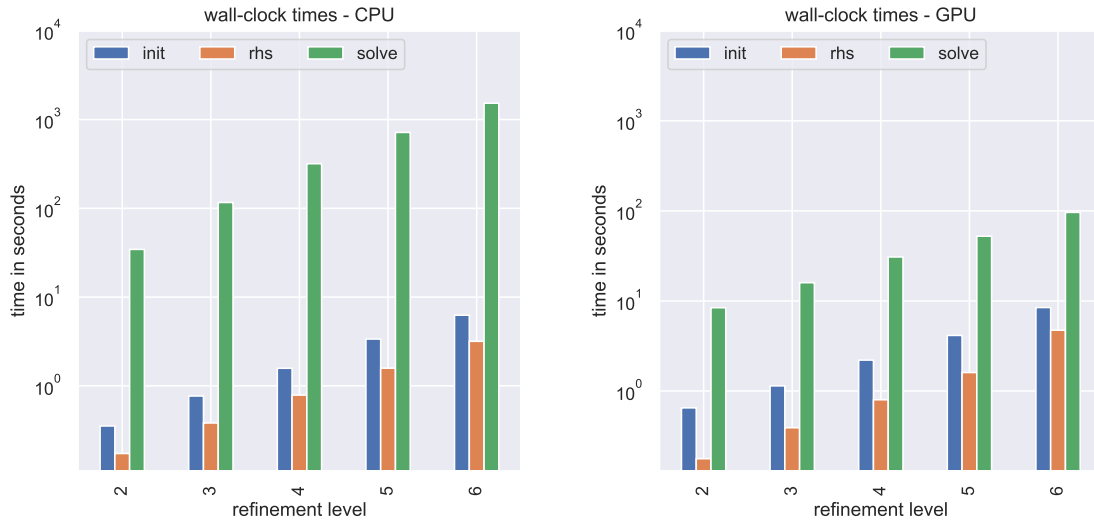
Table 5.2: Elasticity problem: Number of mesh nodes on different mesh levels (first sub-row) and fraction of nodes that are hanging nodes (second sub-row). From top to bottom we show the different adaptive refinement types, compare Fig. 5.3.

Fig. 5.4b shows the scaling of the implementation with respect to the refinement. Note that the meshes are refined locally. Therefore, the number of multigrid levels increases in each step but the overall number of unknowns grows only slowly (not by a factor of 8 that would be expected on a 3d hexahedral mesh). Hence more and more unstructured features and hanging nodes appear on higher mesh levels. Due to the slow growth in the number of degrees of freedoms, the run-times on CPU and GPU increase only slowly with each refinement level, compare also Table 5.2. The results show very good efficiency of the GPU multigrid solver on locally refined meshes with no negative impact of having more and more hanging nodes and less regular structure in the problem.

Next we compare the performance of the GPU implementation on the different types of adaptive mesh shown in Fig. 5.3 with number of unknowns indicated in Table 5.2. The complexity of these mesh types is very different. While the number of nodes increases like 4^l (l is the mesh level) for face refinement, which is typical for 2d problems, and 2^l for the edge refinement, the typical behavior for 1d problems, the scaling is much slower for the vertex-refinement.



(a) Refinement towards edge on mesh level 6, logarithmic scale (left) and linear scale (right).



(b) Refinement towards edge on a sequence of locally refined meshes.

Figure 5.4: Elasticity problem. Wall-clock times on CPU and GPU.

Figure 5.5 shows that the efficiency of the GPU parallelization is robust. On the finest mesh level belonging to the vertex-case in Table 5.3c, the computational time of the solver only drops from 139s on the CPU to 30s on the GPU, a factor of about 4.5. However, this problem has just 25 000 unknowns and is too small to properly utilize a GPU. It is important to note that the GPU parallelization does not lead to an overhead at any point, which negatively affects the entire computing time.

5.3 Navier-Stokes equations

As third example, we consider the time-dependent Navier-Stokes equations in their dimensionless form

$$\partial_t \mathbf{u} - \frac{1}{\text{Re}} \Delta \mathbf{u} + \text{div}(\mathbf{u} \otimes \mathbf{u}) + \nabla p = 0 \quad \text{in } (0, T] \times \Omega, \quad (8)$$

$$\text{div} \mathbf{u} = 0 \quad \text{in } (0, T] \times \Omega. \quad (9)$$

By $\mathbf{u} : (0, T] \times \Omega \rightarrow \mathbb{R}^3$ we denote the velocity field and by $p : (0, T] \times \Omega \rightarrow \mathbb{R}$ the scalar pressure. In our numerical experiment, we use the driven cavity benchmark problem on the time interval $I = (0, 12]$ and on the three dimensional domain $\Omega = (0, 1) \times (0, 1) \times (0, 2)$. We choose the Reynolds number $\text{Re} = 10^3$ and the boundary conditions

$$\mathbf{u}(t, x, y, z) = \begin{cases} (0, 1, 0)^T & \text{if } x = 1, \\ (0, 0, 0)^T & \text{otherwise.} \end{cases}$$

Homogenous initial condition $\mathbf{u}(0, x, y, z) = \mathbf{u}_0 := \mathbf{0}$ hold at time $t = 0$. We set $\mathbf{V} = [H_0^1(\Omega)]^d$ and $Q := \{q \in L^2(\Omega) : \int_{\Omega} q \, dx = 0\}$. The weak formulation of the time-dependent Navier-Stokes equations in its semi-discrete form is

$$(\partial_t \mathbf{u}, \boldsymbol{\chi}) + \frac{1}{\text{Re}} (\nabla \mathbf{u}, \nabla \boldsymbol{\chi}) - (\mathbf{u} \otimes \mathbf{u}, \nabla \boldsymbol{\chi}) - (p, \text{div} \boldsymbol{\chi}) = (\mathbf{f}, \boldsymbol{\chi}) \quad \forall \boldsymbol{\chi} \in \mathbf{V}, \quad (10)$$

$$(\text{div} \mathbf{u}, \xi) = 0 \quad \forall \xi \in Q. \quad (11)$$

Here, we used the divergence form of the convective term once integrated, i.e.

$$(\mathbf{u} \cdot \nabla \mathbf{u}, \boldsymbol{\chi}) = (\text{div}(\mathbf{u} \otimes \mathbf{u}), \boldsymbol{\chi}) = -(\mathbf{u} \otimes \mathbf{u}, \nabla \boldsymbol{\chi}).$$

This representation will be crucial for an efficient realization on the GPU, since in the discrete setting $(\mathbf{u} \otimes \mathbf{u}, \nabla \boldsymbol{\chi})$ can be approximated by sparse matrix vector products, as will be explained shortly.

For the spatial discretization of (10)-(11), we employ finite elements with the inf-sup stable \mathbb{Q}_1 -iso- $\mathbb{Q}_2/\mathbb{Q}_1$ pair. We consider a shape regular mesh Ω_h of the domain and its equidistant refinement $\Omega_{h/2}$. The discrete spaces $\mathbf{V}_h \subset \mathbf{V}$ and $Q_h \subset Q$ consist of \mathbb{Q}_1 polynomials in each cell of $\Omega_{h/2}$ and Ω_h , respectively. The semi-discrete problem is obtained with $\mathbf{u}_h, \boldsymbol{\chi}_h \in \mathbf{V}_h$ and $p_h, \xi_h \in Q_h$. Application of an implicit time discretization for this semi-discrete problem requires fixed point iterations due to the nonlinear transport term. Each iteration step for linearization requires thereby to resolve a nonsymmetric, indefinite system matrix owing to the transport term and the saddle point structure that arises from velocity pressure coupling. Here, we follow an semi-implicit approach where the momentum equation is discretized explicitly.

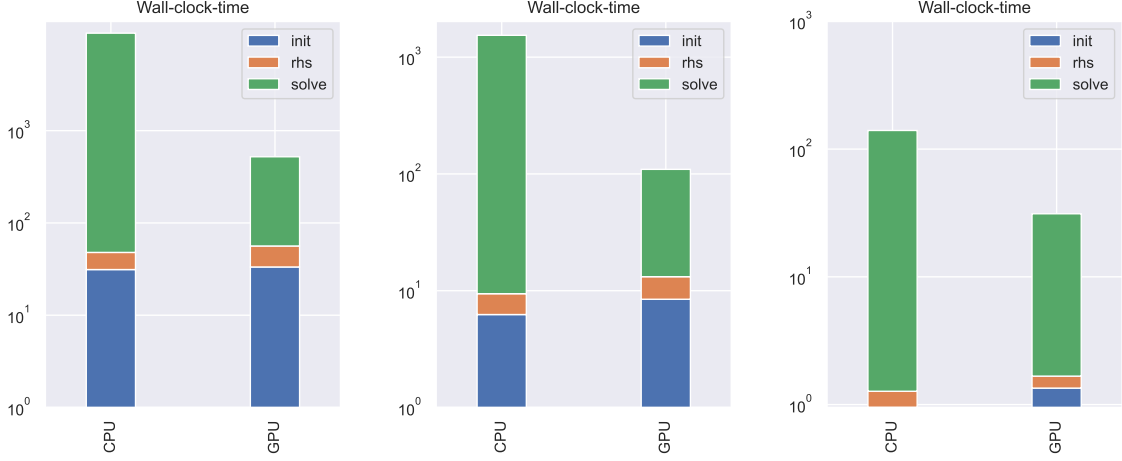


Figure 5.5: Comparison of the refinement types (from left to right): 5 refinements towards one face (left), 6 refinements towards one edge (middle), 6 refinements towards one vertex (right).

Due to better stability and the advantageous diagonal structure, we employ a lumped mass matrix, i.e. we approximate

$$(\mathbf{v}_h, \phi_i)_{i=1}^N \approx M_h^l \mathbf{v}, \quad (12)$$

where $\phi_i^h : \Omega \rightarrow \mathbb{R}$ are the \mathbb{Q}_1 basis functions, $\mathbf{v} \in \mathbb{R}^{N_{nodes} \times 4}$ is the coefficient vector, and M_h denotes the lumped mass matrix given by

$$M_h^l = \text{diag}(m_1, \dots, m_{N_{dof}}), \quad m_i = \sum_j (\phi_j, \phi_i).$$

Moreover, we apply a mass lumping approach also in the nonlinear term, which enables us to implement the convective term as a matrix-vector product with a pre-assembled sparse matrix, see also [19]. In particular, let $\mathcal{I}_h : \mathbf{V} \rightarrow \mathbf{V}_h$ be the nodal interpolation operator. For each $\mathbf{v}_h, \chi_h \in \mathbf{V}_h$, we approximate

$$\begin{aligned} (\text{div}(\mathbf{v}_h \otimes \mathbf{v}_h), \chi_h) &= -(\mathbf{v}_h \otimes \mathbf{v}_h, \nabla \chi_h) \\ &\approx -(\mathcal{I}_h(\mathbf{v}_h \otimes \mathbf{v}_h), \nabla \chi_h) =: n(\mathbf{v}_h \otimes \mathbf{v}_h, \chi_h). \end{aligned} \quad (13)$$

In finite element notation, this discrete approximation amounts to

$$\mathcal{I}_h(\mathbf{v}_h \otimes \mathbf{v}_h) = \sum_i (\mathbf{v}_i \otimes \mathbf{v}_i) \phi_i^h \approx \left(\sum_i \mathbf{v}_i \phi_i^h \right) \otimes \left(\sum_j \mathbf{v}_j \phi_j^h \right).$$

Note that in the interpolation nodes it holds that

$$\mathcal{I}_h(\mathbf{v}_h \otimes \mathbf{v}_h)(\mathbf{x}_k) = \mathbf{v}_h(\mathbf{x}_k) \otimes \mathbf{v}_h(\mathbf{x}_k).$$

The error caused by mass lumping in the zeroth-order term (12) and the convective term (13) are of the same order as the polynomial approximation error and therefore do not effect the error asymptotics. This approach is sometimes denoted as ‘fully practical finite element method’ [3] as it allows for error estimates that reflect the full error including numerical quadrature.

mesh level	DOFs	CPU				GPU			
		init	rhs	solve	sum	init	rhs	solve	sum
2	17 550	0.18	0.07	10.53	10.78	0.47	0.07	4.01	4.55
3	67 686	0.53	0.27	59.58	60.38	0.89	0.28	9.03	10.21
4	263 166	2.10	1.08	371.11	374.29	2.82	1.09	26.23	30.15
5	1 035 030	6.99	4.24	2138.02	2149.25	8.63	7.40	111.69	127.71

(a) Refinements towards a face of the domain.

mesh level	DOFs	CPU				GPU			
		init	rhs	solve	sum	init	rhs	solve	sum
3	24 774	0.77	0.38	116.34	117.49	1.14	0.39	15.96	17.49
4	51 414	1.58	0.79	318.16	320.52	2.20	0.80	30.79	33.79
5	104 358	3.37	1.58	716.25	721.20	4.14	1.60	52.36	58.10
6	209 910	6.25	3.18	1529.04	1538.46	8.45	4.74	96.27	109.45

(b) Refinement towards an edge of the domain.

mesh level	DOFs	CPU				GPU			
		init	rhs	solve	sum	init	rhs	solve	sum
3	11 622	0.45	0.18	40.58	41.21	0.70	0.17	11.56	12.43
4	15 246	0.63	0.23	62.27	63.12	0.92	0.23	15.63	16.78
5	18 870	0.78	0.28	99.26	100.31	1.12	0.28	23.11	24.51
6	22 494	0.95	0.32	138.59	139.86	1.35	0.32	29.5	31.17

(c) Refinement towards a vertex.

Table 5.3: Elasticity problem: measured values for the wall clock times on CPU and GPU on different refinement types.

For the convective term we assemble three sparse matrices

$$C_{h,\{x,y,z\}} = (\phi_j, \partial_{\{x,y,z\}} \phi_i)_{i,j=1}^{N_{nodes}},$$

for the three components x, y, z and compute the three vectors

$$\mathbf{v}_{i,c}^1 = \mathbf{u}_{i,1} \mathbf{u}_{i,c}, \quad \mathbf{v}_{i,c}^2 = \mathbf{u}_{i,2} \mathbf{u}_{i,c}, \quad \mathbf{v}_{i,c}^3 = \mathbf{u}_{i,3} \mathbf{u}_{i,c}, \quad . \quad (14)$$

for $c = 1, 2, 3$, $i = 1, \dots, N_{nodes}$. The residual can then be evaluated using matrix-vector products as

$$-(\mathbf{u}_h \otimes \mathbf{u}_j, \nabla \chi)_{i=1}^{N_{nodes}} \approx -C_{h,x} \mathbf{v}^1 - C_{h,x} \mathbf{v}^2 - C_{h,x} \mathbf{v}^3. \quad (15)$$

The computation of the component-wise products in 14 is not a standard operation that can be expressed in linear algebra. We will therefore require custom kernels to assemble these vectors efficiently on the GPU.

Algorithm 5.1: The fully discrete solution procedure for the Navier-Stokes equations

Given \mathbf{u}_0 . Set $q_h^0 := 0$ and choose $p_h^0 \in Q_h$ s.t. (16) is fulfilled. For $m = 1, \dots, N$ calculate

Step 1: Find $\mathbf{u}_h^m \in \mathbf{V}_h$ such that

$$\frac{1}{k}(\mathbf{u}_h^m, \chi)_* = (\mathbf{f}^{m-1} + \frac{1}{k}\mathbf{u}_h^{m-1}, \chi)_* - A((\mathbf{u}_h^{m-1}, p_h^{m-1} + q_h^{m-1}); (\chi, 0)) \quad \forall \chi \in \mathbf{V}_h.$$

Step 2: Find $q_h^m \in S_h$ such that

$$(\nabla q_h^m, \nabla \varphi) = -\frac{1}{k}(\operatorname{div} \mathbf{u}_h^m, \varphi) \quad \forall \varphi \in S_h.$$

Step 3: Find $p_h^m \in Q_h$ such that

$$(p_h^m, \varphi)_* = (p_h^{m-1} + q_h^m, \varphi)_* - (\nu \operatorname{div} \mathbf{u}_h^m, \varphi) \quad \forall \varphi \in Q_h.$$

5.3.1 Explicit projection solver

Let $k > 0$ be a time step and $N = T/k$. We set $t_n := n \cdot k$ for $0 \leq n \leq N$ and

$$A((\mathbf{u}, p); (\chi, \xi)) := -\nu(\nabla \mathbf{u}, \nabla \chi) + n(\mathbf{u} \otimes \mathbf{u}, \chi) - (p, \operatorname{div} \chi) + (\xi, \operatorname{div} \mathbf{u}).$$

The fully discrete solution algorithm we employ solves the momentum equation explicitly and updates the pressure field by solving a Poisson problem (see Alg. 5.1). Hence, we introduce the solution space $S = H^1(\Omega)$ and its discrete counterpart S_h that consists of \mathbb{Q}_1 polynomials on each cell T of Ω_h . These type of predictor-corrector methods for approximating incompressible flows requires an initial pressure field which must be calculated from the Poisson equation if the right hand side and initial velocity are not zero

$$(\nabla p_h^0, \nabla \varphi) = -(f^0, \nabla \varphi) + ((\mathbf{u}_0 \cdot \nabla) \mathbf{u}_0, \nabla \varphi) + (\nu \Delta \mathbf{u}_0, \varphi)_\Gamma \quad \forall \varphi \in S_h. \quad (16)$$

For justification and well-posedness of this equation, see [18]. Moreover, note that the velocity solutions \mathbf{u}_h^m are so-called predictor solutions. The corrector velocities were eliminated as described in [16].

We set $\Delta t = 10^{-4}$ and consider $(N_x, N_y, N_z) = (32, 32, 64)$ elements in each coordinate direction. The mesh coordinates (x_i, y_j, z_k) for $i \in \{0, \dots, N_x\}$, $j \in \{0, \dots, N_y\}$ and $k \in \{0, \dots, N_z\}$ are defined as

$$\begin{aligned} x_i &= \frac{1}{2} \left(1 + \cos \left(\frac{i \cdot \pi}{N_x} \right) \right), & i &\in \{0, \dots, N_x\}, \\ y_j &= \frac{1}{2} \left(1 + \cos \left(\frac{j \cdot \pi}{N_y} \right) \right), & j &\in \{0, \dots, N_y\}, \\ z_k &= 1 + \sin \left(\frac{(k - N_z) \cdot \pi}{2N_z} \right), & k &\in \{0, \dots, N_z\}. \end{aligned}$$

The meshes contain anisotropic elements. Therefore, to obtain better robustness, we again embed the geometric multigrid solver as preconditioner in the GMRES method.

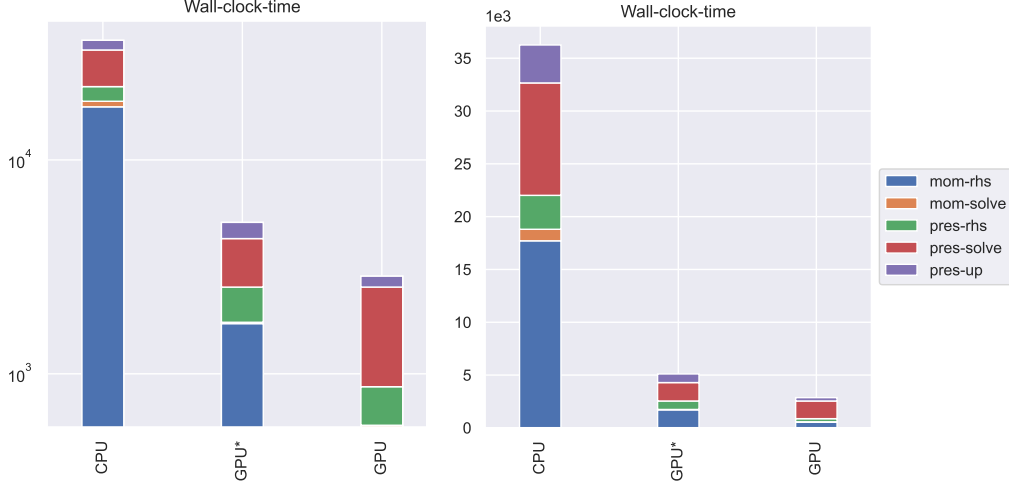


Figure 5.6: Navier-Stokes problem: Wall-clock times CPU vs. GPU (GPU* is without custom kernels), logarithmic scale (left) and linear scale (right). Table 5.4 gives the raw numbers and it also depicts the time required for transfer of data between CPU and GPU.

5.3.2 GPU realization

The explicit pressure correction scheme in Algorithm 5.1 consists largely of the same parts that have already been used for the nonstationary linear problems that have been presented above. The multigrid method is fully run on the GPU as well as all parts of the GMRES solver that work with global matrices and vectors scaling with the dimension of the finite element space. **Step 1** and **Step 3** are explicit and only require sparse matrix vector products as well as inversion of the lumped mass matrix. This however is already stored as a diagonal matrix containing the inverse elements such that standard cuSPARSE methods can be used.

An operation that is not easily expressed in cuBLAS or cuSPARSE is the local assembly of the outer products $\mathbf{u}_i \otimes \mathbf{u}_i \in \mathbb{R}^{3 \times 3}$ in (14). To understand the effect this has on the performance, the numerical results below show two versions: one, simply denoted by (GPU), where a custom CUDA kernel is used to evaluate (14) directly on the GPU and an intermediate version, denoted as (GPU*), where we compute these products on the CPU. This requires transferring the solution vector back and forth whenever this matrix-vector product is required. We add this intermediate results to demonstrate the importance of minimizing memory transfers.

We also use custom kernels for efficiently computing the products with the rectangular matrices corresponding to the discretization of the gradient of the pressure and the divergence of the velocity that is required in preprocessing.

5.3.3 Numerical Results

Fig. 5.6 and Table 5.4 show the overall wall-clock times for the three implementations: CPU using 8 parallel threads, GPU* solely with cuSPARSE, and the GPU version with custom kernels as described in Sec. 5.3.2.

We split the timings into several components. **momentum** corresponds to **Step 1** of Algorithm 5.1. Here, **mom rhs** is the assembly of the right hand side, which we further split into

	CPU	GPU*	GPU
mom-rhs-nonlin	11543.2	966.3	346.4
mom-rhs-p	3381.6	644.0	107.5
mom-rhs-visc	2570.2↓	105.4↓	108.1↓
mom-rhs	17711.3	1717.2	563.4
mom-solve	1091.3↓	24.5↓	11.4↓
momentum	18803.5	1742.2	575.2
pres-rhs	3213.8	801.9	295.6
pres-solve	10643.1↓	1743.7↓	1674.1↓
pres	13857.5	2545.9	1969.9
pres-up.rhs	3180.5	784.7	282.8
pres-up.solve	350.7↓	32.0↓	32.9↓
pres-up	3595.4	817.3	316.2
sum	36527.1	5178.6	2938.9
copy	–	887.1	10.2

Table 5.4: Navier-Stokes problem: Wall-clock times (in seconds) shown in Fig. 5.6. CPU is the times on a CPU using 8 threads. GPU* is the result of the implementation using cuSPARSE without further custom kernel code. GPU includes further optimizations described in Sec. 5.3.2 using custom kernels. For both GPU timings, the code remaining on the CPU is run using 8 parallel threads. The timings for **Step 1** (momentum equation), **Step 2** (pressure Poisson problem) and **Step 3** (pressure update) are split into their contributions. Furthermore we indicate the times for copying data between CPU and GPU. These times are already included in **Step 1**, **Step 2** and **Step 3**.

mom-rhs-nonlin, the multiplication with C_h , compare (15), into **mom-rhs-p** which is a multiplication with a rectangular matrix acting on the pressure and finally into **mom-rhs-visc** that covers the matrix-vector product representing the viscous term. Finally, **mom-solve** is the multiplication with the inverse mass matrix. The assembly of the right hand side is the most costly part in the algorithm. Porting it to the GPU reduces the computational cost by a factor of 10. Here, a substantial further reduction of computational time is reached by introducing custom kernels that preprocess the solution vector for assembling the outer products (14) and for handling rectangular matrices, compare Section 5.3.2. The reduction of computational time is due to saving memory transfer between CPU and GPU, compare columns GPU* and GPU in Table 5.4.

pres covers **Step 2** of Algorithm 5.1, the pressure Poisson problem. Again, we split the timings into **pres-rhs** for the assemble of the right hand side, a sparse matrix vector product computing the divergence of the velocity prediction and **pres-solve** which is the actual inversion of the Laplace problem using the GMRES multigrid solver.

pres-up finally corresponds to **Step 3**, the explicit update of the pressure. Here, **pres-up-rhs** is the assemble of the right hand side and **pres-up-solve** the inversion of the lumped pressure space mass matrix.

Memory is only transfered for initialization (first copy of matrices and vectors) as well as for

the GMRES solver. Here however, only single floats, e.g. results of scalar products or short matrices used in the GMRES orthogonalization must be copied. Their dimension is in the order of number of GMRES steps (always less than 10).

By combining all optimizations the overall runtime for the $12/\Delta t = 12\,000$ time steps is reduced from about 37 000 s (about 10 h) using 8 CPU cores to about 3 000 s (about 50 min) with the GPU, i.e. we obtain a speedup by a factor of approximately 12.

6 Conclusions

In this paper, we presented a GPU parallelization of the adaptive finite element library Gascoigne 3d. Our implementation uses primarily the cuBLAS and cuSPARSE libraries, which directly map dense and sparse linear algebra operations that arise as part of the adaptive finite element computations to the GPU. The use of cuBLAS and cuSPARSE covers most cases of relevance and leads to code with only small differences between CPU and GPU versions. We also demonstrated that custom CUDA kernels can provide significant speedups, e.g. for the assembly of terms such as right-hand-sides. Data transfer to and from the GPU is encapsulated by developing custom implementations for Gascoigne 3d's data interfaces. Combining these features, we achieved that large parts are consecutively computed on the GPU, so that only infrequent data transfers between CPU and GPU are necessary and these are not significant bottlenecks.

Our approach is conceptually simple, since largely only existing linear algebra operations are mapped to the GPU, and requires only limited CUDA expertise. Correspondingly, also the implementation effort for the GPU-parallelization is limited and also substantially simplifies to simultaneously support a CPU and a GPU backend in the code base in the future. The option to directly also integrated custom CUDA kernels provides at the same time great flexibility and has helped us in to substantially reduce the data transfer between CPU and GPU, that otherwise easily become a bottleneck.

In future work, we want to extend our GPU parallelization of Gascoigne 3d further. The most important step to reach the full flexibility is to realize the quadrature of variational formulations, i.e. the assembly of matrices and residuals, directly on the GPU. An interesting alternative to native CUDA is the use of the high-performance linear algebra libraries that are the backends of machine learning frameworks such as torch and jax, for example torch inductor or XLA. These provide flexible support for a range of accelerators, e.g. also TPUs, and also compilers that optimize the computations for the available compute hardware. Triton is also an interesting intermediate ground between native CUDA and higher level libraries.

The code of our implementation will be made available upon publication.

Acknowledgments

UK, ML and TR acknowledge the support of the GRK 2297 MathCoRe, funded by the Deutsche Forschungsgemeinschaft, Grant Number 314838170.

References

- [1] Hartwig Anzt, Terry Cojean, Goran Flegar, Fritz Göbel, Thomas Grützmacher, Pratik Nayak, Tobias Ribizel, Yuhsiang Mike Tsai, and Enrique S. Quintana-Ortí. Ginkgo: A

- Modern Linear Operator Algebra Framework for High Performance Computing. *ACM Transactions on Mathematical Software*, 48(1):2:1–2:33, February 2022.
- [2] W. Bangerth, R. Hartmann, and G. Kanschat. deal.ii—a general-purpose object-oriented finite element library. *ACM Trans. Math. Softw.*, 33(4):24–es, 2007.
 - [3] J. W. Barrett, J. F. Blowey, and H. Garcke. On fully practical finite element approximations of degenerate Cahn-Hilliard systems. *ESAIM: M2AN*, 35(4):713 – 748, 2001.
 - [4] R. Becker and M. Braack. Multigrid techniques for finite elements on locally refined meshes. *Numerical Linear Algebra with Applications*, 7:363–379, 2000. Special Issue.
 - [5] R. Becker, M. Braack, and T. Richter. Parallel multigrid on locally refined meshes. In W. Jäger, R. Rannacher, and J. Warnatz, editors, *Reactive Flows, Diffusion and Transport*, pages 77–92. Springer Berlin Heidelberg, 2006.
 - [6] R. Becker and R. Rannacher. An optimal control approach to a posteriori error estimation in finite element methods. In A. Iserles, editor, *Acta Numerica 2001*, volume 37, pages 1–225. Cambridge University Press, 2001.
 - [7] Kaifeng Bi, Lingxi Xie, Hengheng Zhang, Xin Chen, Xiaotao Gu, and Qi Tian. Accurate medium-range global weather forecasting with 3D neural networks. *Nature*, 2023.
 - [8] M. Braack and T. Richter. Solutions of 3d Navier-Stokes benchmark problems with adaptive finite elements. *Computers and Fluids*, 35(4):372–392, 2006.
 - [9] M. Braack and T. Richter. Solutions of 3D Navier-Stokes benchmark problems with adaptive finite elements. *Computers and Fluids*, 35(4):372–392, May 2006.
 - [10] Malte Braack, Roland Becker, Dominik Meidner, Thomas Richter, and Boris Vexler. The finite element toolkit Gascoigne, 2021.
 - [11] James Bradbury, Roy Frostig, Peter Hawkins, Matthew James Johnson, Chris Leary, Dougal Maclaurin, George Necula, Adam Paszke, Jake VanderPlas, Skye Wanderman-Milne, and Qiao Zhang. JAX: composable transformations of Python+NumPy programs, 2018.
 - [12] D.R. Castillo, U. Kaya, and T. Richter. A explicit time integration method for the boussinesq approximation, 2024. arXiv preprint.
 - [13] M. Geveler, D. Ribbrock, D. Göddeke, P. Zajac, and S. Turek. Towards a complete FEM-based simulation toolkit on GPUs: Unstructured grid finite element geometric multigrid solvers with strong smoothers based on sparse approximate inverses. *Computers & Fluids*, 80:327–332, 2013.
 - [14] Dominik Goddeke, Sven H.M. Buijssen, Hilmar Wobker, and Stefan Turek. GPU acceleration of an unmodified parallel finite element Navier-Stokes solver. In *2009 International Conference on High Performance Computing & Simulation*, pages 12–21, 2009.
 - [15] Dominik Göddeke, Robert Strzodka, Jamaludin Mohd-Yusof, Patrick McCormick, Hilmar Wobker, Christian Becker, and Stefan Turek. Using GPUs to improve multigrid solver performance on a cluster. *Int. J. Comput. Sci. Eng.*, 4(1):36–55, 2008.

- [16] Jean-Luc Guermond. Some implementations of projection methods for Navier-Stokes equations. *ESAIM: Mathematical Modelling and Numerical Analysis*, 30(5):637–667, 1996.
- [17] Vincent Heuveline, Dimitar Lukarski, Nico Trost, and Jan-Philipp Weiss. *Parallel Smoothers for Matrix-Based Geometric Multigrid Methods on Locally Refined Meshes Using Multicore CPUs and GPUs*, pages 158–171. Springer Berlin Heidelberg, 2012.
- [18] John G. Heywood and Rolf Rannacher. Finite element approximation of the nonstationary Navier–Stokes problem. i. regularity of solutions and second-order error estimates for spatial discretization. *SIAM Journal on Numerical Analysis*, 19(2):275–311, 1982.
- [19] U. Kaya and T. Richter. Local pressure-correction and explicit time integration for incompressible flows. submitted.
- [20] M. Kimmritz and T. Richter. Parallel multigrid method for finite element simulations of complex flow problems on locally refined meshes. *Numerical Linear Algebra with Applications*, 18:615–636, 2011.
- [21] B. N. Lawrence, M. Rezný, R. Budich, P. Bauer, J. Behrens, M. Carter, W. Deconinck, R. Ford, C. Maynard, S. Mullerworth, C. Osuna, A. Porter, K. Serradell, S. Valcke, N. Wedi, and S. Wilson. Crossing the chasm: how to develop weather and climate models for next generation computers? *Geoscientific Model Development*, 11(5):1799–1821, 2018.
- [22] M. Naumov, M. Arsaev, P. Castonguay, J. Cohen, J. Demouth, J. Eaton, S. Layton, N. Markovskiy, I. Regulý, N. Sakharnykh, V. Sellappan, and R. Strzodka. Amgx: A library for gpu accelerated algebraic multigrid and preconditioned iterative methods. *SIAM Journal on Scientific Computing*, 37(5):S602–S626, 2015.
- [23] NVIDIA. cublas api reference guide. <https://docs.nvidia.com/cuda/cublas>. Accessed: 2024-04-09.
- [24] NVIDIA. cuSPARSE library documentation, 2022.
- [25] Christian Obrecht, Frédéric Kuznik, Bernard Tourancheau, and Jean-Jacques Roux. Multi-GPU implementation of the lattice Boltzmann method. *Computers & Mathematics with Applications*, 65(2):252–261, 2013. Special Issue on Mesoscopic Methods in Engineering and Science (ICMMES-2010, Edmonton, Canada).
- [26] Adam Paszke, Sam Gross, Soumith Chintala, Gregory Chanan, Edward Yang, Zachary DeVito, Zeming Lin, Alban Desmaison, Luca Antiga, and Adam Lerer. Automatic differentiation in pytorch. In *NIPS 2017 Autodiff Workshop*, 2017.
- [27] Dirk Ribbrock, Markus Geveler, Dominik Göddeke, and Stefan Turek. Performance and accuracy of Lattice-Boltzmann kernels on multi- and manycore architectures. *Procedia Computer Science*, 1(1):239–247, 2010. ICCS 2010.
- [28] T. Richter. *Fluid-structure Interactions. Models, Analysis and Finite Elements*, volume 118 of *Lecture Notes in Computational Science and Engineering*. Springer, 2017.
- [29] Dustin Ruda, Stefan Turek, Dirk Ribbrock, and Peter Zajac. Very fast finite element Poisson solvers on lower precision accelerator hardware: A proof of concept study for Nvidia

- Tesla V100. *The International Journal of High Performance Computing Applications*, 36(4):459–474, 2022.
- [30] Y. Saad. *Iterative Methods for Sparse Linear Systems*. PWS Publishing Company, 1996.
- [31] Amit Sabne. Xla : Compiling machine learning for peak performance, 2020.
- [32] N. Sakharlykh. High-performance geometric multi-grid with GPU acceleration, 2016. NVIDIA Technical Blog.
- [33] R. Stevenson. An optimal adaptive finite element method. *SNA*, 42(5):2188–2217, 2005.
- [34] Inc. The Khronos Group. SYCL: a cross-platform abstraction layer for heterogeneous computing, 2021. Accessed: 2024-05-06.
- [35] Philippe Tillet, H. T. Kung, and David Cox. Triton: an intermediate language and compiler for tiled neural network computations. In *Proceedings of the 3rd ACM SIGPLAN International Workshop on Machine Learning and Programming Languages*, page 10–19, New York, NY, USA, 2019. Association for Computing Machinery.
- [36] Christian R. Trott, Damien Lebrun-Grandie, Daniel Arndt, Jan Ciesko, Vinh Dang, Nathan Ellingwood, Rahulkumar Gayatri, Evan Harvey, Daisy S. Hollman, Dan Ibanez, Nevin Liber, Jonathan Madsen, Jeff Miles, David Poliakoff, Amy Powell, Sivasankaran Rajamanickam, Mikael Simberg, Dan Sunderland, Bruno Turcksin, and Jeremiah Wilke. Kokkos 3: Programming model extensions for the exascale era. *IEEE Transactions on Parallel and Distributed Systems*, 33(4):805–817, apr 2022.